



Generation of whistler waves by continuous HF heating of the upper ionosphere

A. Vartanyan, G. M. Milikh, B. Eliasson, A. C. Najmi, Michel Parrot, K. Papadopoulos

► To cite this version:

A. Vartanyan, G. M. Milikh, B. Eliasson, A. C. Najmi, Michel Parrot, et al.. Generation of whistler waves by continuous HF heating of the upper ionosphere. *Journal of Nuclear and Radiochemical Sciences*, 2016, 51 (7), pp.1188-1198 <10.1002/2015RS005892>. <insu-01372250>

HAL Id: insu-01372250

<https://insu.hal.science/insu-01372250v1>

Submitted on 29 May 2017

HAL is a multi-disciplinary open access archive for the deposit and dissemination of scientific research documents, whether they are published or not. The documents may come from teaching and research institutions in France or abroad, or from public or private research centers.

L'archive ouverte pluridisciplinaire **HAL**, est destinée au dépôt et à la diffusion de documents scientifiques de niveau recherche, publiés ou non, émanant des établissements d'enseignement et de recherche français ou étrangers, des laboratoires publics ou privés.



HAL Authorization

RESEARCH ARTICLE

10.1002/2015RS005892

Special Section:

Ionospheric Effects
Symposium 2015

Key Points:

- First clear observations of LH-whistler conversion by ionospheric HF heating
- Both linear and nonlinear mechanisms for LH-whistler conversion are observed
- LH-whistler mode conversion simulations confirm the experimental observations

Correspondence to:

A. Vartanyan,
aram.a.vartanyan@gmail.com

Citation:

Vartanyan, A., G. M. Milikh, B. Eliasson, A. C. Najmi, M. Parrot, and K. Papadopoulos (2016), Generation of whistler waves by continuous HF heating of the upper ionosphere, *Radio Sci.*, 51, 1188–1198, doi:10.1002/2015RS005892.

Received 13 DEC 2015

Accepted 1 JUL 2016

Accepted article online 7 JUL 2016

Published online 29 JUL 2016

Generation of whistler waves by continuous HF heating of the upper ionosphere

A. Vartanyan¹, G. M. Milikh², B. Eliasson^{2,3}, A. C. Najmi¹, M. Parrot⁴, and K. Papadopoulos²
¹ Johns Hopkins University Applied Physics Laboratory, Laurel, Maryland, USA, ² Department of Physics and Astronomy, University of Maryland, College Park, Maryland, USA, ³ Department of Physics, University of Strathclyde, Glasgow, UK, ⁴ Laboratoire de Physique et Chimie de l'Environnement et de l'Espace, CNRS, Orleans, France

Abstract Broadband VLF waves in the frequency range 7–10 kHz and 15–19 kHz, generated by *F* region CW HF ionospheric heating in the absence of electrojet currents, were detected by the DEMETER satellite overflying the High Frequency Active Auroral Research Program (HAARP) transmitter during HAARP/BRIOCHE campaigns. The VLF waves are in a frequency range corresponding to the *F* region lower hybrid (LH) frequency and its harmonic. This paper aims to show that the VLF observations are whistler waves generated by mode conversion of LH waves that were parametrically excited by HF-pump-plasma interaction at the upper hybrid layer. The paper discusses the basic physics and presents a model that conjectures (1) the VLF waves observed at the LH frequency are due to the interaction of the LH waves with meter-scale field-aligned striations—generating whistler waves near the LH frequency; and (2) the VLF waves at twice the LH frequency are due to the interaction of two counterpropagating LH waves—generating whistler waves near the LH frequency harmonic. The model is supported by numerical simulations that show good agreement with the observations. The (Detection of Electromagnetic Emissions Transmitted from Earthquake Regions) results and model discussions are complemented by the Kodiak radar, ionograms, and stimulated electromagnetic emission observations.

1. Introduction

The generation of electromagnetic waves in the ELF/VLF frequency range by modulated HF heating of the ionospheric plasma has been the subject of many studies. Experiments and theory revealed that three completely different physical processes control their generation: (1) electrojet current modulation, which relies on modulated HF heating of the D/E region plasma electrons in the presence of electrojet currents, capable of VLF generation up to 10–20 kHz [Rietveld *et al.*, 1986; Barr *et al.*, 1985; Papadopoulos and Chang, 1985; Papadopoulos *et al.*, 1990, 2003, 2005; Platino *et al.*, 2004, 2006; Piddychiy *et al.*, 2008; Cohen *et al.*, 2011; Cohen and Golkowski, 2013]; (2) ionospheric current drive [Papadopoulos *et al.*, 2011a, 2011b], which relies on modulated heating of the electron temperature in the *F* region, is independent of the presence of electrojet currents and capable of ELF generation up to 60 Hz; and (3) excitation of the thermal cubic nonlinearity is an additional electrojet-independent mechanism for generating ELF/VLF waves [Moore *et al.*, 2013].

The objective of this paper is to present observations of a fourth mechanism that generates broadband ($\Delta f/f \approx 0.1$ –0.25) VLF waves in the frequency range 7–10 kHz and 15–19 kHz, which were detected by the DEMETER (Detection of Electromagnetic Emissions Transmitted from Earthquake Regions) satellite during *F* region CW HF ionospheric heating experiments at HAARP, in the absence of electrojet currents. Note that the VLF waves are in a frequency range corresponding to the *F* region lower hybrid (LH) frequency and its second harmonic. We believe this is no accident; in this paper, we aim to show that the VLF waves must have been generated by LH-to-whistler mode conversion, where the LH waves were parametrically excited by HF-pump-plasma interactions at the upper hybrid (UH) layer. We will discuss the basic physics and present a model that conjectures (1) the interaction of the LH waves with meter-scale field-aligned striations generates whistlers at the LH frequency and (2) the interaction of two counterpropagating LH waves generates whistlers at twice the LH frequency. The model is supported by numerical simulations that are in good agreement with the observations.

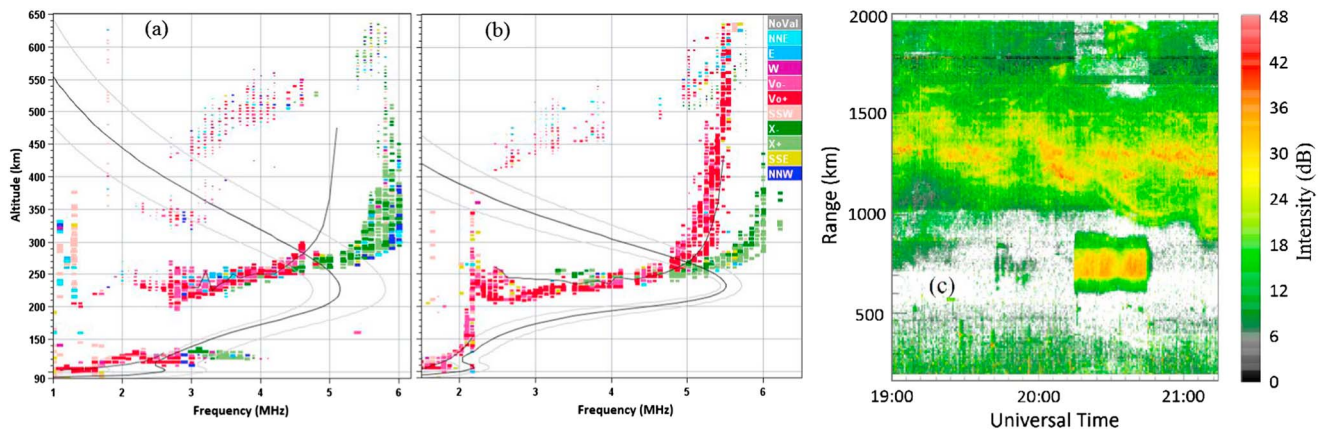


Figure 1. Ionograms (a) during Experiment 1 and (b) during Experiment 2 showing a smooth ionosphere with sporadic E layer present, as well as Kodiak radar observations (c) during Experiment 1 showing strong reflections (given in decibel) during the time of heating (20:15–20:45 UT) in the range 700–800 km.

2. Experimental Observations

We report below the results of two daytime High Frequency Active Auroral Research Program (HAARP)/BRIOCHE experiments conducted during flyovers of DEMETER, which travels at a speed of about 7.5 km/s at an altitude of 670 km. In both experiments HAARP operated at its maximum power of 3.6 MW with O mode, and the HF beam directed along the magnetic zenith (MZ). We utilized the DEMETER Instrument Champ Electrique (ICE) [Berthelier *et al.*, 2006b], which measured one component of the electric field in the VLF range at a sampling rate of 40 kHz, and the Instrument Sonde de Langmuir [Berthelier *et al.*, 2006a], which measured the electron density at a sampling rate of 1 Hz. Ground diagnostics included stimulated electromagnetic emission (SEE) observations, the on-site ionosonde and magnetometer, and the Kodiak coherent radar; ionograms helped select the heating frequency. One experiment was conducted on 16 October 2009 20:15–20:45 UT (Experiment 1), during a quiet daytime ionosphere with $f_0F_2 = 5.15$ MHz and a moderate sporadic E layer present, as shown by the ionogram in Figure 1a; HAARP operated at CW with a frequency of $f_H = 5.1$ MHz, corresponding to reflection altitude $h_r = 220$ km, while the closest approach of the DEMETER satellite to the HAARP MZ was $\Delta R = 69$ km. The other experiment was conducted on 2 October 2010 20:15–20:34 UT (Experiment 2), during a quiet daytime ionosphere with $f_0F_2 = 5.5$ MHz and a prominent E layer presented, as shown by Figure 1b; HAARP operated with 0.7 Hz square pulse modulation rather than CW, with $f_H = 4.25$ MHz (just below the third gyroharmonic, 4.35 MHz), $h_r = 200$ km, and $\Delta R = 40$ km. The key parameters of the experiments described above are summarized in Table 1. Both experiments were conducted during weak-to-moderate D/E region absorption and a steady ground magnetometer reading of about 10 nT. While not available during Experiment 2, the Kodiak radar did operate during Experiment 1; its observations, shown in Figure 1c, reveal significant reflections during heating in the range 700–800 km, indicating the buildup of strong plasma striations.

The experimental results are shown in Figures 2 and 3. Figures 2a and 2b show spectrograms observed by ICE during DEMETER flyovers of HAARP during the experiments; time is measured relative to the closest approach of the MZ, corresponding to 20:33:00 UT for Experiment 1 and 20:27:47 UT for Experiment 2. The spectrograms were computed directly from the ICE waveform data using a short-time Fourier transform, with a window size of 4096 points and 50% overlap. In both figures VLF signals are observed in the vicinity of the MZ over approximately 10 s, corresponding to a flyover distance of 75 km. Note that the regular temporal structure of the VLF waves in Figure 2b is attributable to the 0.7 s on-off square pulse HF heating, while the irregular structure in Figure 2a could be attributed to ducted whistler propagation [Woodroffe *et al.*, 2013]. Note that the

Table 1. Key Experimental Information, Including the HF Frequency (f_H) and Reflection Height (h_r), the Critical Frequency (f_0F_2) and Critical Height (h_mF_2), the Closest Approach of DEMETER to the HAARP MZ (ΔR), and the E-W Half-Power Beam Width at the Heating Altitude (L_{EW}), and the HF Heating Setting

Experiment Label	Heating Time (UT)	f_H (MHz)/ h_r (km)	f_0F_2 (MHz)/ h_mF_2 (km)	ΔR (km)/ L_{EW} (km)	HF heating setting
1	10/16/2009 20:15–20:45	5.1/220	5.15/225	69/32	CW
2	02/10/2010 20:15–20:34	4.25/200	5.5/230	40/39	Modulated at 0.7 Hz

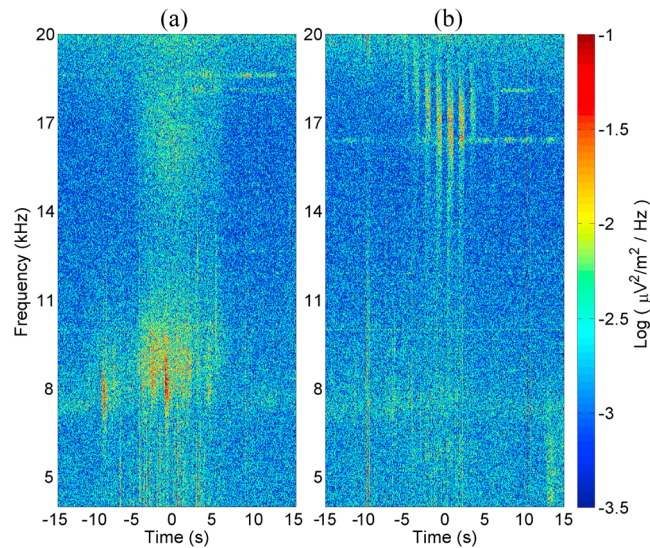


Figure 2. Spectrogram seen by DEMETER (a) during Experiment 1 on 16 October 2009 in which HAARP used CW heating and (b) during Experiment 2 on 2 October 2010 in which HAARP used 0.7 Hz square pulse modulated heating. In both cases time = 0 corresponds to the closest approach of DEMETER to the HAARP magnetic zenith.

spectrograms contain features that are not related to our experiments: a faint band at ~ 7 – 8 kHz stretching across the entire time domain, corresponding to naturally occurring LH oscillations; broadband and temporally narrow spectral features outside of the heated region; and narrowband signals (e.g., at 16.5 and 18.5 kHz) due to man-made transmissions.

We should remark that it would be ideal to instead present spectrograms for the VLF magnetic field, in order to facilitate the interpretation of whistler waves in the observations; unfortunately, the DEMETER magnetic field instrument is unusable due to instrumental interference and noise. Figure 3 shows the power spectral density (PSD) for the two experiments, measured near the closest approach to the HAARP MZ. For Experiment 1 (Figure 3a) the central frequencies are at 8.2 kHz and 16.5 kHz, corresponding to the F region LH frequency and its harmonic, with full width at half maximum (FWHM) of approximately 2 kHz and 3 kHz. For Experiment 2 (Figure 3b) the central frequency is near 16.8 kHz, close to the LH harmonic, and has a 2 kHz FWHM.

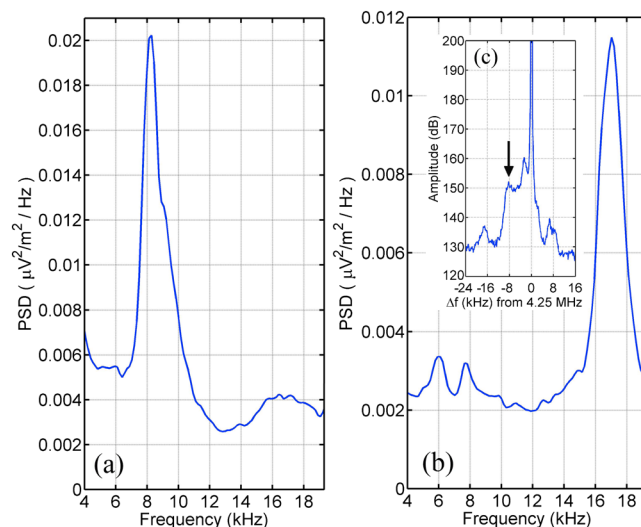


Figure 3. Power spectral density versus frequency measured on 16 October 2009 (Figure 2a) and on 2 October 2010 (Figure 2b), obtained from a 2 s average of the Figure 2 observations near the closest approach of the MZ. SEE spectrum observed on the ground at HAARP on 2 October 2010 (Figure 3c); Δf is the observed frequency relative to the pump frequency.

Note that the peak near 8 kHz in Figure 3b is of natural origin, as mentioned above. However, the peak at 6 kHz is apparently due to the HAARP heating, as it is only present near time = 0; the reader may look for the 6 kHz feature in the spectrogram Figure 2b; however, it is very faint and may be difficult to see. This unknown spectral feature is beyond the scope of this paper and as such is left for future work. The PSDs in Figures 3a and 3b were obtained by applying Welch's method to the waveform data using a window size of 4096 points and 50% overlap; for Experiment 1 the PSD was obtained from a 2 s interval of the data near time = 0, while for Experiment 2 the PSD was obtained by averaging PSDs of the three "on-times" closest to time = 0. In addition to the standard diagnostics, SEE measurements were available during Experiment 2. The inserted Figure 3c shows the SEE spectrum observed on the ground at HAARP, with the field amplitude in decibel versus Δf —the observed frequency relative to the pump frequency. The large central peak at $\Delta f = 0$ is the backscattered pump wave, while the smaller peak (marked by the arrow) that is shifted down by about 8.5 kHz from the pump is the so-called downshifted maximum (DM). The SEE spectrum additionally shows a smaller second downshifted maximum (2DM)—downshifted by twice the former or about 17 kHz. However, it is important to note that the presence of a 2DM is not a necessity for our model that we are presenting below; the presence of the DM alone is sufficient, as it indicates that LH waves—which are necessary for the self-consistency of our model—were definitely present in the heated region. The details of the SEE, DM, and LH waves, their mutual connection, and their relevance to whistler generation are discussed extensively in the following sections.

In addition to VLF detected by DEMETER, we looked for simultaneous measurements of VLF on the ground, which was being collected at the Sinona Creek VLF site in Chistochina, AK; there was no detection by the VLF receivers (Robert Moore, private communication, 2015), presumably due to significant attenuation of the whistlers during their penetration toward the ground. The reason for this could be caused by the effect discussed in Shao *et al.* [2012] that whistlers experience a strong attenuation in the ionosphere at the height 90–150 km. The attenuation is due to the conversion between whistler and LH waves in the presence of short-scale natural field-aligned density irregularities. The latter are associated with large-scale structures such as sporadic *E* layer or so-called quasi periodic structures. In fact, sporadic *E* layer was detected during one of the experiments (see Figures 1a and 1b). Low amplitudes coupled with the fact that the generated VLF waves are very broadband, makes their detectability on the ground very difficult; detection of signals below the noise threshold via time integration requires a signal that is coherent and narrowband, which is *not* the case according to the observations in Figures 2 and 3. We also attempted to obtain ground VLF measurements collected by Stanford University, but unfortunately, the data from 2009 to 2010 were unavailable due to server issues (George Jin, private communication, 2015).

2.1. Possibility of Electrostatic (ES) Wave Observations

In lieu of moving further, we should briefly comment on the possibility of our observations being ES waves rather than whistlers; the following considerations highlight our reasons for believing that the observed VLF waves are indeed whistlers.

ES wave detection by DEMETER is only possible if the said ES waves propagated 450 km from the HF-heated region to the DEMETER altitude; this hypothesis has two major issues: (1) ES waves are localized to near the HF-heated region and have not been observed to travel significantly outside this region. (2) The only known ES wave that could be a candidate for this hypothesis is the LH wave, which has a frequency of about 8 kHz, as observed in Experiment 1; however, *both* Experiment 1 and Experiment 2 observe VLF at the LH second harmonic (16–17 kHz)—a frequency range for which there exists no known pump-induced ES plasma wave. The only process that is consistent with the observations is the linear and nonlinear conversion of LH waves in the heated region to whistlers that propagate to DEMETER, the details of which are discussed throughout the remainder of the paper. Because we can think of no plausible alternative, we will be interpreting these observations as whistler mode waves.

3. Discussion and Theoretical Considerations

The observed VLF waves are in a frequency range corresponding to the *F* region LH frequency and its second harmonic. In this section we motivate that the observations are due to mode conversion of LH waves to whistler waves, where the LH waves were parametrically excited by HF-pump-plasma interactions at the UH layer. Moreover, in examining the observations presented in Figures 2 and 3 we find a major peculiarity: while in Experiment 1 VLF waves were measured at the LH frequency and its second harmonic, in Experiment

2 VLF waves appeared only at the second harmonic. To understand this puzzling absence and subsequent theoretical discussions, it pays to first review the HF-pump-plasma interactions in the heated region.

3.1. Parametric Excitation of LH Waves at the UH Resonance

As an O mode HF wave of frequency f_0 is transmitted along the MZ, it propagates to the reflection point slightly below the height where the wave frequency matches the plasma frequency, $f_0 = f_{pe}$. Along the way, it additionally encounters the upper hybrid resonance (UHR) $f_0^2 = f_{pe}^2 + f_{ce}^2$, where f_{ce} is the electron gyrofrequency.

At the UHR, the HF pump wave mode converts to UH waves on natural or self-focusing-driven irregularities [Mjølhus, 1998; Gondarenko et al., 2005; Eliasson and Papadopoulos, 2015], trapping and amplifying the UH waves until parametric instabilities are triggered [Gurevich, 2007] that excite LH waves. The LH wave is manifested by the DM in the SEE spectrum and has been confirmed by numerous SEE observations. Several theoretical models [e.g., Shvarts and Grach, 1997] have been proposed for DM generation, culminating in models that naturally explain the regularly observed multiple DM features (2DM, 3DM, ...). One such model is summarized by the following.

A dipole EM pump wave (EM_{pump}) of frequency f_0 is mode converted on plasma density striation (D) and excites UH waves of the same frequency, which become trapped inside the striations,

$$EM_{\text{pump}}(f_0) + D \rightarrow UH(f_0, \pm k), \quad (1)$$

where k is the typical perpendicular wave number of the trapped UH wave; for the sake of brevity some of the components (e.g., parallel components) have been left out for these set of interactions but will be discussed below when relevant. Once an UH wave reaches a threshold amplitude, it parametrically decays by the three-wave process into another UH wave (UH_1) and a LH wave of frequency f_l and perpendicular wave number k_l ,

$$UH(f_0, k) \rightarrow UH_1(f_0 - f_l, k - k_l) + LH(f_l, k_l) \quad (2)$$

The UH_1 wave, which is downshifted from the pump by the LH frequency, can interact with irregularities and mode convert back to EM waves that are then observed on the ground in the SEE spectrum as a DM (EM_{DM}),

$$UH_1(f_0 - f_l, k - k_l) + D \rightarrow EM_{\text{DM}}(f_0 - f_l) \quad (3)$$

This process can continue iteratively,

$$UH_1(f_0 - f_l, k - k_l) \rightarrow UH_2(f_0 - 2f_l, k - 2k_l) + LH(f_l, k_l) \quad (4)$$

$$UH_2(f_0 - 2f_l, k - 2k_l) + D \rightarrow EM_{2\text{DM}}(f_0 - 2f_l) \quad (5)$$

and generate several DMs (2DM, 3DM, ...), with each new one further downshifted by the LH frequency from the previous. A set of interactions analogous to the above will generate counterpropagating LH waves with wave number $-k_l$. One should note that there are small but nonzero parallel wave vector components of the UH waves, and hence the generated LH waves, due to the finite wavelength of the EM wave and due to the large-scale plasma inhomogeneity [Mjølhus, 1998; Eliasson and Papadopoulos, 2015]; this has been omitted here but will be discussed below for the generation of whistler waves by LH waves.

The above set of interactions shows why the presence of a DM in SEE observations is crucial for the consistency of our model; the presence of a DM is a proxy of parametrically excited LH waves, which are a prerequisite for generation of whistler waves in our model. In fact, the DM feature in Figure 3c is downshifted by about 8.5 kHz, indicating that LH waves near said frequency were present in the heated region.

3.2. Striation Development and the Missing LH Peak

Several theoretical and experimental studies [Bell and Ngo, 1990; Eliasson and Papadopoulos, 2008; Shao et al., 2012; Vaskov et al., 1998] have shown that LH waves can be converted into whistler waves (W) (and vice versa) in the presence of static meter-scale plasma density striations (D):

$$LH(f_l, \pm k_{l,\perp}, k_{l,\parallel}) + D(0, \mp k_{\text{str}}, 0) \rightarrow W(f_l, 0, k_{l,\parallel}), \quad (6)$$

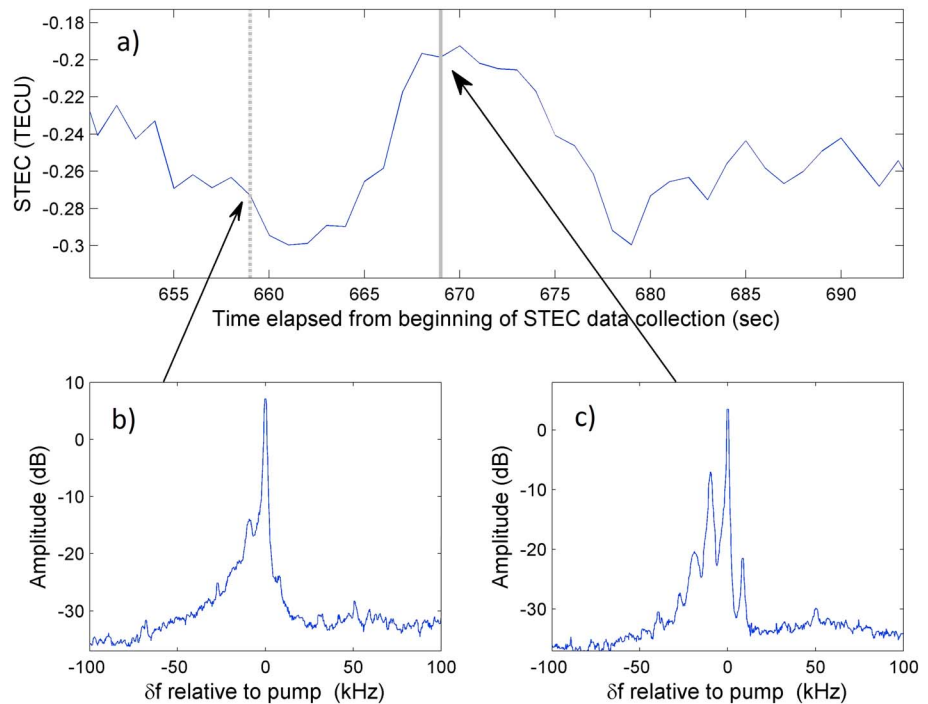


Figure 4. (a) Measurements of STEC during an HF heating experiment; variation in STEC has a timescale of several seconds. (b) Simultaneously, SEE was measured 20 ms after the start of heating, already showing signs of DM. (c) SEE after 10 s of heating shows well-developed DM, along with 2DM and 3DM.

where we are now explicitly showing the \perp symbol and have included the parallel component of the wave vectors for clarity. Following the start of HF heating, the development of the DM (and hence LH waves) has been shown to be less than 20 ms [Sergeev *et al.*, 2013], while the development of significant meter-scale-sized striations take much longer: on the order of 5–10 s [Honary *et al.*, 2011]. These times scales can be demonstrated by an experiment we conducted at HAARP, with conditions similar to those in Experiment 2 (daytime, quiet ionosphere, $f_H = 5.75$ MHz $\approx 4f_{ce}$, $h_r = 200$ km, pulsed MZ heating). SEE measurements and GPS slant total electron content (STEC) data were simultaneously collected. The results are presented in Figure 4 and show SEE with a well-developed DM and simultaneously an increase in STEC, corresponding to the formation of plasma density striations [Milikh *et al.*, 2008]. The STEC had a buildup time of about 5–10 s (Figure 4a), while the buildup time of the DM was under 20 ms (Figure 4b) and became fully developed with multiple DM features after about 10 s (Figure 4c). These differences in time scales explain the missing peak near the LH frequency in Figure 3b. Namely, recall the main difference between the two experiments: Experiment 1 used CW heating, while Experiment 2 used pulsed heating with on/off times of 0.7 s. Figures 4a and 4b illustrate that using short heating pulses with 0.7 s on and 0.7 s off, such as in Experiment 2, is enough to generate LH waves but does not allow for the development of significant artificial striations. Without a sufficient buildup of striations, the linear mode conversion mechanism would be too inefficient to be observed by DEMETER, which is consistent with the absence of VLF near the LH frequency in Figure 3b.

3.3. Whistler Waves at the Second LH Harmonic

The main peak in Figure 3a near the LH frequency is naturally explained by the fact that CW heating generates meter-scale striations necessary for LH-whistler conversion. Our attention now shifts to the LH second harmonic in Figures 3a and 3b. LH waves with a frequency near (or greater than) twice the LH frequency cannot exist, since this would break the LH regime requirement $|\pi/2 - \theta| < \sqrt{m_e/m_i}$, where θ is the angle between the LH wave vector and the background geomagnetic field, \mathbf{B}_0 . Thus, the second harmonic must be generated from a different kind of interaction, presumably a nonlinear one.

We suggest that the mechanism responsible for VLF waves near the second LH harmonic is due to the nonlinear interaction of oppositely propagating LH waves that generate whistlers at the LH harmonic, analogous

to counterpropagating Langmuir waves interacting to give EM waves with twice the Langmuir frequency [Akimoto *et al.*, 1988]:

$$\text{LH}(f_l, +k_{l,\perp}, k_{l,\parallel}) + \text{LH}(f_l, -k_{l,\perp}, 0) \rightarrow W(2f_l, 0, k_{l,\parallel}), \quad (7)$$

where the parallel component of the wave vector has been included for clarity; note that we have set one of the LH waves to be fully perpendicular (but not both), in anticipation of our simulation setup that is described below. This nonlinear mechanism does not directly rely on striations but instead relies on the density fluctuations due to the large amplitude LH electric field.

We consider one perpendicularly (to the magnetic field) propagating LH wave with wave number $k_{l,\perp} = k_{\perp 1}$ and the frequency ω_{l1} given by the lower hybrid resonance frequency (for $\omega_{pe} \gg \omega_{ce}$)

$$\omega_{l1}^2 = \omega_{ce}\omega_{ci} \quad (8)$$

and one obliquely propagating LH wave with wave vector components $k_{\perp 2} = -k_{\perp 1}$ and $k_{\parallel 2}$ and frequency ω_{l2} given by

$$\omega_{l2}^2 = \frac{\omega_{ce}\omega_{ci}k_{\perp 2}^2 + \omega_{ce}^2k_{\parallel 2}^2}{k_{\perp 2}^2 + k_{\parallel 2}^2}. \quad (9)$$

The beating of these two waves gives rise to a whistler wave with parallel wave number $k_{w\parallel} = k_{\parallel 2}$ and frequency

$$\omega_w = \frac{c^2k_{w\parallel}^2}{\omega_{pe}^2}\omega_{ce} = \frac{c^2k_{\parallel 2}^2}{\omega_{pe}^2}\omega_{ce} \quad (10)$$

The frequency condition $\omega_w = \omega_{l1} + \omega_{l2}$ then gives

$$\frac{c^2k_{\parallel}^2}{\omega_{pe}^2} = \sqrt{\frac{m_e}{m_i}} + \sqrt{\frac{k_{\perp}^2 m_e / m_i + k_{\parallel}^2}{k_{\perp}^2 + k_{\parallel}^2}}, \quad (11)$$

which relates k_{\parallel} to k_{\perp} (having now dropped the subscript 2 for brevity). Finally, setting $k_{\parallel} = k_0 \cos(\theta)$ and $k_{\perp} = k_0 \sin(\theta)$ gives

$$\cos(\theta) = \frac{\omega_{pe}}{ck_0} \left(2\sqrt{\frac{m_e}{m_i}} + \left(1 - \frac{m_e}{m_i} \right) \frac{\omega_{pe}^2}{c^2k_0^2} \right)^{1/2} \quad (12)$$

As an example, the LH wave number $k_0 = 4\text{m}^{-1}$ and $\omega_{pe} = 3.1 \times 10^7\text{s}^{-1}$ gives $\cos(\theta) \approx 0.0029$, i.e., the propagation angle is almost (but not exactly) perpendicular to the ambient magnetic field. The whistler wave frequency for this case will be $\omega_w = 1.15 \times 10^5\text{s}^{-1}$, corresponding to $f_w = 18\text{kHz}$.

3.4. LH-Whistler Mode Conversion: Model and Simulations

Eliasson and Papadopoulos [2008] studied LH-whistler mode conversion in the presence of plasma density striations by formulating the problem into two coupled equations, corresponding to the whistler and LH wave. This was achieved by first deriving one equation for the electron particle current and subsequently taking the $|\lambda_e^2 \nabla^2| \ll 1$ and $|\lambda_e^2 \nabla^2| \gg 1$ limits to obtain two coupled equations for the whistler particle current (\mathbf{j}_w) and LH particle current (\mathbf{j}_{LH}), respectively:

$$\frac{\partial \mathbf{j}_w}{\partial t} = -\frac{e\lambda_e^2}{m_e} (1 - \lambda_e^2 \nabla^2)^{-1} \nabla \times [\nabla \times ((n_{\text{str}} + n_{\text{LH}})\mathbf{E}_{\text{LH}} + \mathbf{j}_w \times \mathbf{B}_0)], \quad (13)$$

$$\frac{\partial \mathbf{j}_{\text{LH}}}{\partial t} = \nabla^{-2} \left\{ \frac{e}{m_e} \nabla \times [\nabla \times (n_{\text{str}}\mathbf{E}_w + \mathbf{j}_{\text{LH}} \times \mathbf{B}_0)] - \frac{e}{m_i} \nabla [\nabla \cdot (\mathbf{j}_{\text{LH}} \times \mathbf{B}_0)] \right\}, \quad (14)$$

where $\lambda_e = c/\omega_{pe}$ is the electron inertial length. The whistler and LH electric fields were shown to be given by [Eliasson and Papadopoulos, 2008]

$$\mathbf{E}_w = -(\mathbf{j}_w \times \mathbf{B}_0)/n_0 \quad (15)$$

$$\mathbf{E}_{\text{LH}} = -\nabla [\nabla^{-2} [\nabla \cdot (\mathbf{j}_{\text{LH}} \times \mathbf{B}_0)] / n_0], \quad (16)$$

where \mathbf{B}_0 is the background magnetic field vector, n_0 is the constant background plasma density, and n_{str} accounts for external density striations. Thus, in the presence of density striations the LH electric field can drive whistler waves and vice versa. Note that n_{LH} , which is the density fluctuation of the LH wave, was neglected in *Eliasson and Papadopoulos* [2008] during linearization of the equations. We generalized the model by keeping this nonlinear coupling, for reasons that will become clear below. The density fluctuations are obtained from the continuity equation

$$\frac{\partial n_{\text{LH}}}{\partial t} + \nabla \cdot \mathbf{j}_{\text{LH}} = 0. \quad (17)$$

Eliasson and Papadopoulos [2008] showed that efficient resonant mode conversion from LH to whistler waves occurs when the striation full width (D_{str}) is comparable to half the perpendicular wavelength of the LH wave:

$$D_{\text{str}} \sim \frac{\pi}{k_{\perp, \text{LH}}}. \quad (18)$$

During this resonant mode conversion process the LH and whistler waves have the same frequency, $\omega_l = \omega_w = \omega$; the wave vector components along the geomagnetic field are the same for the LH and whistler wave $k_{\parallel, \text{LH}} = k_{\parallel, \text{wh}} = k_{\parallel}$, but their perpendicular components $k_{\perp, \text{LH}}$ and $k_{\perp, \text{wh}}$ can be different. While the LH wave propagates almost perpendicular to the magnetic field, the whistler wave propagates primarily along the magnetic field but can be slightly oblique. For the discussions in this paper, parallel whistler propagation ($k_{\perp, \text{wh}} = 0$) is a reasonable approximation and will be assumed below. With these conditions the LH and whistler dispersion relations give

$$\omega_l^2 = \omega^2 = \frac{\omega_{l,0}^2 k_{\perp, \text{LH}}^2 + \omega_{ce}^2 k_{\parallel}^2}{k_{\perp, \text{LH}}^2 + k_{\parallel}^2} \approx \frac{\omega_{l,0}^2 k_{\perp, \text{LH}}^2 + \omega_{ce}^2 k_{\parallel}^2}{k_{\perp, \text{LH}}^2} \quad (19)$$

$$\omega_w^2 = \omega^2 = \lambda_e^4 k_{\parallel}^2 (k_{\perp, \text{wh}}^2 + k_{\parallel}^2) \omega_{ce}^2 \approx \lambda_e^4 k_{\parallel}^4 \omega_{ce}^2 \quad (20)$$

where $\omega_{l,0} = 2\pi f_{l,0} = \sqrt{\omega_{ce}\omega_{ci}}$ is the LH oscillation frequency. Eliminating k_{\parallel}^2 in equation (19) by using equation (20), we then obtain

$$k_{\perp, \text{LH}}^2 = \frac{\omega_{ce}\omega}{\lambda_e^2(\omega^2 - \omega_{l,0}^2)} = \frac{\sqrt{m_i/m_e}(f/f_{l,0})}{\lambda_e^2[(f/f_{l,0})^2 - 1]} \quad (21)$$

Since the ionosphere has more than one ion species, m_i should be interpreted as an effective ion mass. By using the 2007 International Reference Ionosphere (IRI), we can estimate the local plasma parameters necessary for finding $k_{\perp, \text{LH}}$ from equation (21). We take the electron gyrofrequency to be $f_{ce} = 1.45$ MHz near altitudes of 200–220 km at HAARP [Mahmoudian et al., 2013]. For typical ionospheric conditions, such as in Experiments 1 and 2, the IRI model gives $f_{l,0} \approx 7.5$ kHz, $\lambda_e \approx 9$ m. If we take $f = 8.2$ kHz, corresponding to the main peak in Figure 3a, then equation (21) gives an approximate range of $k_{\perp, \text{LH}} \approx 3\text{--}4$ m^{−1} for the relevant altitudes. The corresponding resonant striation width can be found from equation (18) to be $D_{\text{str}} \approx 1$ m, which is the characteristic size of small scale striations known to exist during continuous HF heating [Carpenter, 1974].

Consider the model (13)–(17) with input parameters similar to the above estimates. We take $n_0 = 3.1 \times 10^5$ cm^{−3} and assume a Gaussian striation depletion profile $n_{\text{str}} = -n_{0,\text{str}} \exp(-x^2/D^2)$, with a half-width $D = D_{\text{str}}/2 = 0.4$ m and depletion amplitude ($n_{0,\text{str}}$) that is 1.25% of n_0 . Moreover, the initial conditions are set to be three LH wave packets of identical size placed on top of each other in the middle of the simulation domain, where they can mutually interact with each other and the external striation; all wave packets have $k_{\perp, \text{LH}} = 4$ m^{−1}. For the first wave packet, the angle (of the wave vector) relative to \mathbf{B}_0 is set to resonantly generate whistler waves at the LH frequency by (linearly) interacting with the striation [Eliasson and Papadopoulos, 2008]. For the remaining two wave packets: one is set to be exactly perpendicular ($\theta = \pi/2$), while the angle of the other is analogously set (using equation 12) to resonantly generate whistler waves at the LH harmonic by nonlinearly interacting with the perpendicular LH wave packet. Running a simulation with this setup generates mode-converted whistler waves with frequencies that correspond to the LH frequency and its harmonic, as shown in Figure 5. Figure 5a reveals the magnitude of the LH electric field vector, while Figure 5b shows the magnitude of the whistler magnetic field vector. The spectrum of the whistler magnetic field, as seen from a stationary observation point at the top of the simulation domain ($z = 9$ km), is plotted in Figure 5c and shows good agreement with the experimentally observed PSD in Figure 3a. The vertical lines indicate

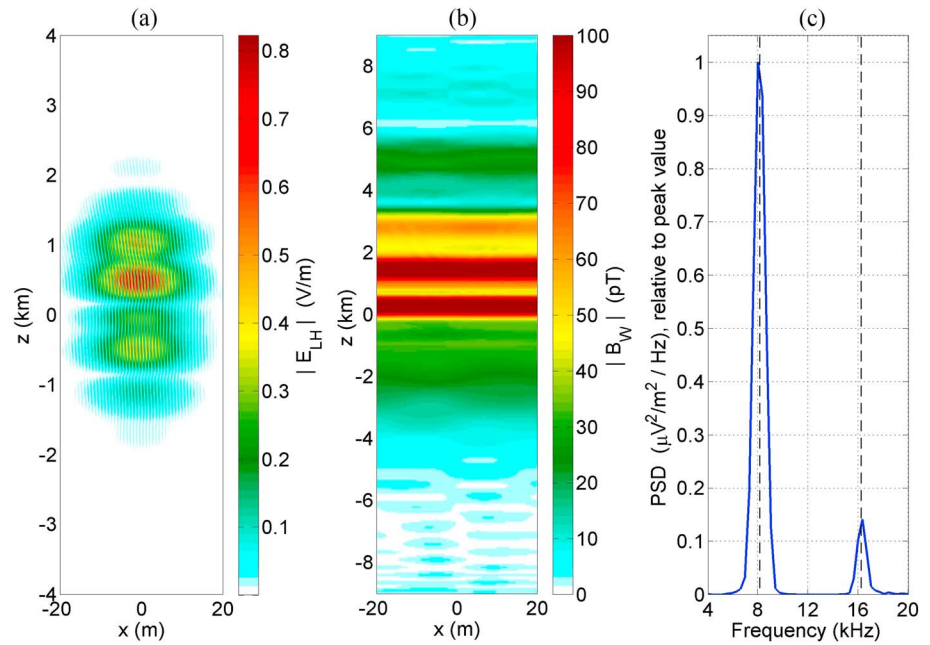


Figure 5. Simulation results showing generation of mode-converted whistler waves with frequencies at the LH frequency and its second harmonic: (a) the magnitude of the LH electric field in V/m, (b) magnitude of the whistler magnetic field in picotesla, and (c) spectrum of the y component whistler electric field, relative to the peak value; the vertical lines in Figure 5c represent the LH frequency and its second harmonic.

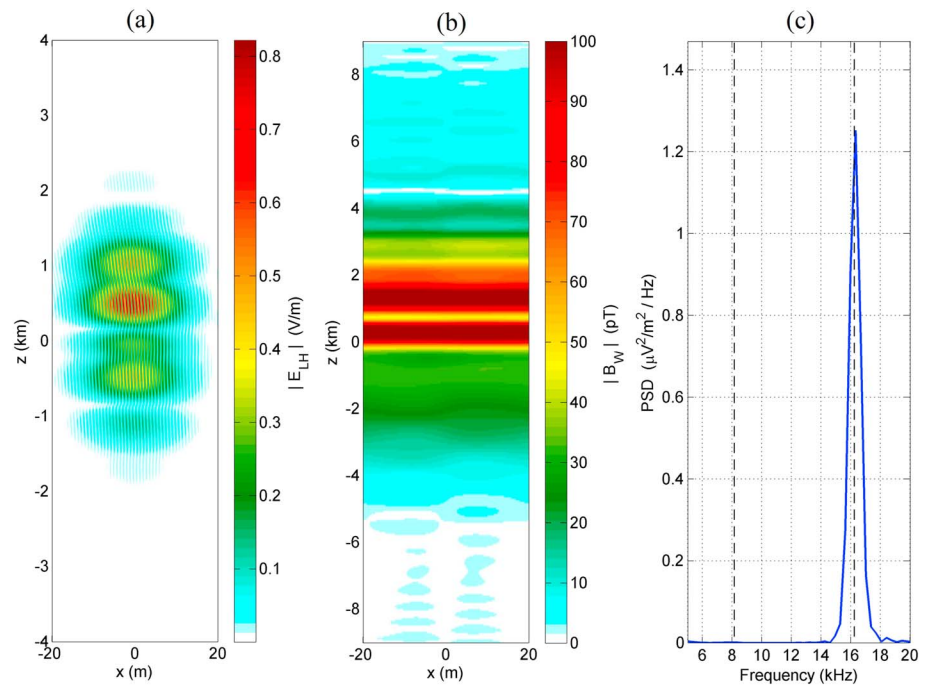


Figure 6. Simulation results showing generation of mode-converted whistler waves with frequency equal to the LH second harmonic: (a) The magnitude of the LH electric field in V/m, (b) magnitude of the whistler magnetic field in picotesla, and (c) spectrum of the y component whistler electric field; the vertical lines in Figure 6c represent the LH frequency and its second harmonic.

the LH frequency and its harmonic, and as expected, they are close to the peaks of the whistler spectrum. If the striation amplitude were set to zero in the above-described simulation setup, we would expect only whistler generation at the LH harmonic. Figure 6 shows the results of such a simulation confirming our expectations and also confirming the VLF spectrum observed by DEMETER in Figure 3b.

4. Conclusions

This paper described two HAARP/DEMETER experiments in which VLF waves of artificial origin were detected by the DEMETER satellite while overflying the HF-heated region of the ionosphere. The observations were shown to be consistent with parametrically excited LH waves being mode converted to whistler waves during HF heating. The VLF near the LH frequency observed during Experiment 1, in which we had used CW HF heating, was shown to be consistent with resonant mode conversion to whistler waves in the presence of artificially pumped meter-scale striations. The VLF near the LH harmonic observed during both Experiment 1 and Experiment 2 was shown to be generated by a different mechanism: due to the nonlinear three-wave interaction of two counter propagating LH waves generating a whistler wave. Simulation results based on the LH-whistler mode conversion model of Eliasson and Papadopoulos [2008] were presented, where a nonlinear coupling term was added to the model. The results of the simulation showed mode-converted whistlers with frequencies near the LH frequency and its harmonic, consistent with the observed spectrum during Experiment 1. It was also shown that the absence of any VLF features near the LH frequency during Experiment 2 was due to the fact that Experiment 2 used pulsed heating, thus not allowing the development of significant meter-scale striations and preventing an efficient linear coupling from LH waves to whistlers. However, the nonlinear coupling—which generates whistlers at the LH harmonic—does not directly rely on striations, which is consistent with the VLF spectrum observed during Experiment 2. The discussed mode conversion mechanisms could be a source for VLF generation in regions where the electrojet is absent.

Acknowledgments

AV and GM were supported by DARPA via a subcontract N684228 with BAE Systems and also by the MURI grant FA95501410019. We are very thankful to Paul Bernhardt, Stan Briczinski and Carl Siefring for sharing their SEE data. We acknowledge CNES for the use of the DEMETER data. We acknowledge very useful discussions with Andrei Demekhov and Lena Titova, and Mike McCarrick's expert help in conducting the HAARP experiments. We are also grateful to Robert Moore for fruitful discussions and taking his time to check ground VLF data. The raw DEMETER VLF data for this letter is available for download via FTP at http://ftp.astro.umd.edu/pub/SPP/GRL_LHwhistler_paper_data/, and Aram Vartanyan (aram.a.vartanyan@gmail.com) may be contacted directly for questions or access to the data.

References

- Akimoto, K., H. L. Rowland, and K. Papadopoulos (1988), Electromagnetic radiation from strong Langmuir turbulence, *Phys. Fluids*, **31**(8), 2185–2189, doi:10.1063/1.866618.
- Barr, R., M. T. Rietveld, H. Kopka, P. Stubbe, and E. Nielsen (1985), Extra-low-frequency radiation from the polar electrojet antenna, *Nature*, **317**, 155–157, doi:10.1038/317155a0.
- Bell, T. F., and H. D. Ngo (1990), Electrostatic lower hybrid waves excited by electromagnetic whistler mode waves scattering from planar magnetic-field-aligned plasma density irregularities, *J. Geophys. Res.*, **95**(A1), 149–172.
- Berthelier, J., M. Godefroy, F. Leblanc, E. Seran, D. Peschard, P. Gilbert, and J. Artru (2006a), IAP, the thermal plasma analyzer on DEMETER, *Planet. Space Sci.*, **54**(5), 487–501, doi:10.1016/j.pss.2005.10.018.
- Berthelier, J. J., et al. (2006b), ICE, the electric field experiment on DEMETER, *Planet. Space Sci.*, **54**(5), 456–471, doi:10.1016/j.pss.2005.10.016.
- Carpenter, G. B. (1974), VHF and UHF bistatic observations of a region of the ionosphere modified by a high power radio transmitter, *Radio Sci.*, **9**(11), 965–969.
- Cohen, M. B., U. S. Inan, D. Piddiyachiy, N. G. Lehtinen, and M. Golkowski (2011), Magnetospheric injection of ELF/VLF waves with modulated or steered HF heating of the lower ionosphere, *J. Geophys. Res.*, **116**, A06308, doi:10.1029/2010JA016194.
- Cohen, M. B., and M. Golkowski (2013), 100 days of ELF/VLF generation via HF heating with HAARP, *J. Geophys. Res. Space Physics*, **118**, 6597–6607, doi:10.1002/jgra.50558.
- Eliasson, B., and K. Papadopoulos (2008), Numerical study of mode conversion between lower hybrid and whistler waves on short-scale density striations, *J. Geophys. Res.*, **113**, A09315, doi:10.1029/2008JA013261.
- Eliasson, B., and K. Papadopoulos (2015), Numerical study of anomalous absorption of O mode waves on magnetic field-aligned striations, *Geophys. Res. Lett.*, **42**(8), 2603–2611, doi:10.1002/2015GL063751.
- Gondarenko, N. A., S. L. Ossakow, and G. M. Milikh (2005), Generation and evolution of density irregularities due to self-focusing in ionospheric modifications, *J. Geophys. Res.*, **110**, A09304, doi:10.1029/2005JA011142.
- Gurevich, A. V. (2007), Nonlinear effects in the ionosphere, *Physics-Uspekhi*, **50**(11), 1091–1121, doi:10.1070/PU2007v050n11ABEH006212.
- Honary, F., N. Borisov, M. Beharrell, and A. Senior (2011), Temporal development of the magnetic zenith effect, *J. Geophys. Res.*, **116**, A06309, doi:10.1029/2010JA016029.
- Mahmoudian, A., W. A. Scales, P. A. Bernhardt, H. Fu, S. J. Briczinski, and M. J. McCarrick (2013), Investigation of ionospheric stimulated Brillouin scatter generated at pump frequencies near electron gyroharmonics, *Radio Sci.*, **48**(6), 685–697, doi:10.1002/2013RS005189.
- Milikh, G., A. Gurevich, K. Zybin, and J. Secan (2008), Perturbations of GPS signals by the ionospheric irregularities generated due to HF-heating at triple of electron gyrofrequency, *Geophys. Res. Lett.*, **35**, L22102, doi:10.1029/2008GL035527.
- Mjølhus, E. (1998), Theoretical model for long time stimulated electromagnetic emission generation in ionospheric radio modification experiments, *J. Geophys. Res.*, **103**(A7), 14,711–14,729, doi:10.1029/98JA00927.
- Moore, R. C., S. Fujimaru, D. A. Kotovsky, and M. Golkowski (2013), Observations of ionospheric ELF and VLF wave generation by excitation of the thermal cubic nonlinearity, *Phys. Rev. Lett.*, **111**(23), 235007, doi:10.1103/PhysRevLett.111.235007.
- Papadopoulos, K., and C. L. Chang (1985), Generation of ELF/VLF waves in the ionosphere by Dynamo processes, *Geophys. Res. Lett.*, **12**(5), 279–282.
- Papadopoulos, K., C. L. Chang, P. Vitello, and A. Drobot (1990), On the efficiency of ionospheric ELF generation, *Radio Sci.*, **25**(6), 1311–1320.
- Papadopoulos, K., T. Wallace, M. McCarrick, G. M. Milikh, and X. Yang (2003), On the efficiency of ELF/VLF generation using HF heating of the auroral electrojet, *Plasma Phys. Reports*, **29**(7), 561–565, doi:10.1134/1.1592554.

- Papadopoulos, K., T. Wallace, G. M. Milikh, W. Peter, and M. McCarrick (2005), The magnetic response of the ionosphere to pulsed HF heating, *Geophys. Res. Lett.*, **32**, L13101, doi:10.1029/2005GL023185.
- Papadopoulos, K., N. A. Gumerov, X. Shao, I. Doxas, and C. L. Chang (2011a), HF-driven currents in the polar ionosphere, *Geophys. Res. Lett.*, **38**, L12103, doi:10.1029/2011GL047368.
- Papadopoulos, K., C. L. Chang, J. Labenski, and T. Wallace (2011b), First demonstration of HF-driven ionospheric currents, *Geophys. Res. Lett.*, **38**, L20107, doi:10.1029/2011GL049263.
- Piddyachiy, D., U. S. Inan, T. F. Bell, N. G. Lehtinen, and M. Parrot (2008), DEMETER observations of an intense upgoing column of ELF/VLF radiation excited by the HAARP HF heater, *J. Geophys. Res.*, **113**, A10308, doi:10.1029/2008JA013208.
- Platino, M., U. S. Inan, T. F. Bell, J. Pickett, E. J. Kennedy, J. G. Trotignon, J. L. Rauch, and P. Canu (2004), Cluster observations of ELF/VLF signals generated by modulated heating of the lower ionosphere with the HAARP HF transmitter, *Ann. Geophys.*, **22**(7), 2643–2653, doi:10.5194/angeo-22-2643-2004.
- Platino, M., U. S. Inan, T. F. Bell, M. Parrot, and E. J. Kennedy (2006), DEMETER observations of ELF waves injected with the HAARP HF transmitter, *Geophys. Res. Lett.*, **33**, L16101, doi:10.1029/2006GL026462.
- Rietveld, M. T., H. Kopka, and P. Stubbe (1986), D-region characteristics deduced from pulsed ionospheric heating under auroral electrojet conditions, *J. Atmos. Terr. Phys.*, **48**(4), 311–326.
- Sergeev, E., S. Grach, a. Shindin, E. Mishin, P. Bernhardt, S. Briczinski, B. Isham, M. Broughton, J. LaBelle, and B. Watkins (2013), Artificial ionospheric layers during pump frequency stepping near the 4th gyroharmonic at HAARP, *Phys. Rev. Lett.*, **110**(6), 65002, doi:10.1103/PhysRevLett.110.065002.
- Shao, X., B. Eliasson, A. S. Sharma, G. Milikh, and K. Papadopoulos (2012), Attenuation of whistler waves through conversion to lower hybrid waves in the low-altitude ionosphere, *J. Geophys. Res.*, **117**, A04311, doi:10.1029/2011JA017339.
- Shvarts, M. M., and S. M. Grach (1997), Interaction of upper and lower hybrid waves and generation of the downshifted maximum feature of stimulated electromagnetic emissions, *J. Atmos. Sol. Terr. Phys.*, **59**(18), 2421–2429, doi:10.1016/S1364-6826(96)00136-8.
- Vaskov, V. V., N. I. Budko, O. V. Kapustina, Y. M. Mikhailov, N. A. Ryabova, G. L. Gdalevich, G. P. Komrakov, and A. N. Maresov (1998), Detection on the Intercosmos-24 satellite of VLF and ELF waves stimulated in the topside ionosphere by the heating facility 'Sura', *J. Atmos. Sol. Terr. Phys.*, **60**(12), 1261–1274, doi:10.1016/S1364-6826(98)00054-6.
- Woodroffe, J. R., A. V. Streltsov, A. Vartanyan, and G. M. Milikh (2013), Whistler propagation in ionospheric density ducts: Simulations and DEMETER observations, *J. Geophys. Res. Space Physics*, **118**, 7011–7018, doi:10.1002/2013JA019445.